Kepler Instrument Performance: an In-flight Update

Douglas A. Caldwell*[a] Jeffrey E. Van Cleve[a] Jon M. Jenkins[a] Vic S. Argabright[b] Jeffery J. Kolodziejczak[c] Edward W. Dunham[d] John C. Geary[e] Peter Tenenbaum[a] Hema Chandrasekaran[a,f] Jie Li[a] Hayley Wu[a] Jason Von Wilpert[g]

[a]SETI Institute/NASA Ames Research Center, MS 244-30, Moffett Field, CA 94035;
[b]Ball Aerospace & Technologies Corp.,1600 Commerce Street, Boulder, CO 80301;
[c]NASA Marshall Space Flight Center, VP60, Huntsville, AL 35812;
[d]Lowell Observatory, 1400 West Mars Hill Road, Flagstaff, AZ 86001;
[e]Smithsonian Astrophysical Observatory, 60 Garden St., Cambridge, MA 02138;
[f] Lawrence Livermore National Laboratory, 7000 East Avenue Livermore, CA 94550-9698;
[g] University of California, Santa Cruz, 1156 High St., Santa Cruz, CA 95064

ABSTRACT

The Kepler Mission is designed to detect the 80 parts per million (ppm) signal from an Earth-Sun equivalent transit. Such precision requires superb instrument stability on time scales up to 2 days and systematic error removal to better than 20 ppm. The sole scientific instrument is the Photometer, a 0.95 m aperture Schmidt telescope that feeds the 94.6 million pixel CCD detector array, which contains both Science and Fine Guidance Sensor (FGS) CCDs. Since Kepler's launch in March 2009, we have been using the commissioning and science operations data to characterize the instrument and monitor its performance. We find that the in-flight detector properties of the focal plane, including bias levels, read noise, gain, linearity, saturation, FGS to Science crosstalk, and video crosstalk between Science CCDs, are essentially unchanged from their pre-launch values. Kepler's unprecedented sensitivity and stability in space have allowed us to measure both short- and long- term effects from cosmic rays, see interactions of previously known image artifacts with starlight, and uncover several unexpected systematics that affect photometric precision. Based on these results, we expect to attain Kepler's planned photometric precision over 90% of the field of view.

Keywords: *Kepler Mission*, exoplanets, space telescopes, photometer, CCD

1. INTRODUCTION

The Kepler Mission has been observing a 115 square degree field of view (FOV) in Cygnus centered at RA = 19h 22m 40s, Dec = 45d 30' since May 2009 in search of transiting extrasolar planets.[1] The primary goal of the Kepler mission is to measure the frequency of Earth-size planets orbiting in the habitable zones of Sun-like stars.[2] In order to meet this goal, the mission uses a wide-field photometer designed to give 20 part per million (ppm) photometric precision on 12th magnitude stars in 6.5 hours over timescales of order 2 days. The instrument also needs to have a very high duty cycle to allow for nearly continuous viewing and to be sufficiently stable over timescales of years so that the precision over 2 day timescales does not degrade significantly. The photometer uses a 0.95 m aperture Schmidt telescope and a focal plane with 42 CCD detectors totaling 96 million pixels on the sky. Details of the instrument design, construction and testing are given elsewhere.[1,3,4] Early results from Kepler indicate that the instrument is performing as designed[5] and that we are getting both the photometric precision and the instrument stability necessary to meet Kepler's goals.[6,7] However, the presence of several image artifacts put some parts of the focal plane at risk to achieving the precision needed to find Earth-size transits[5] Detailed descriptions of the image artifacts as well as mitigation steps that have been developed are given elsewhere.[8]

*douglas.caldwell@nasa.gov

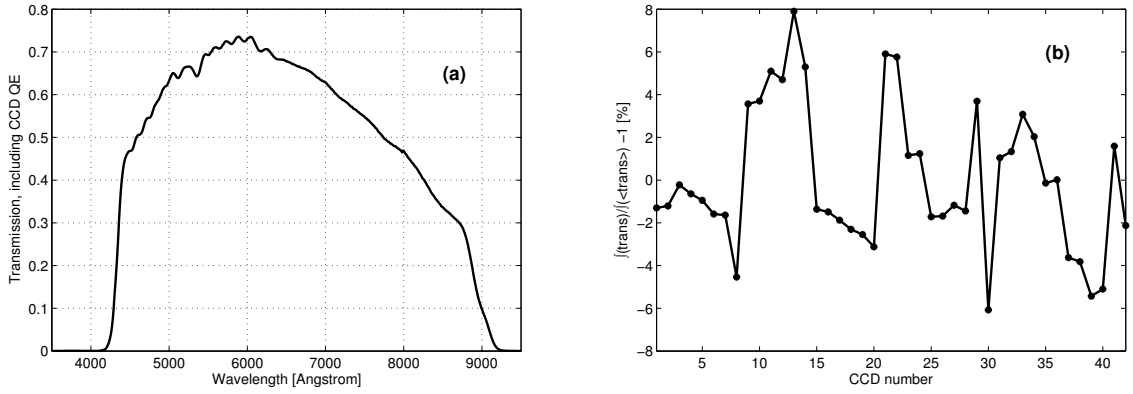

Figure 1: *Kepler* total relative transmission including CCD QE. Panel (a), mean transmission over all channels on the focal plane. Panel (b), relative integrated transmission difference from mean transmission for each of the 42 CCDs. The maximum integrated transmission difference is 8%, not including vignetting, which is up to 11% at the edge of the field of view.

In this paper we give an updated report on the in-flight detector properties after nearly a year of operations for comparison with those found in the *Kepler* Instrument Handbook.[4]

2. TELESCOPE AND OPTICS PERFORMANCE

The *Kepler* spacecraft consists of a Schmidt telescope mounted on the spacecraft bus. The Schmidt telescope consists of a 1.4 m primary mirror, a 0.95 m fused-quartz corrector plate, and 25 sapphire field-flattener lenses (FFL) at the focal plane. The focal length of 1.4 m results in science field-of-view (FOV) of over 115 square degrees and a plate scale of 3.98 arcseconds/pixel. Because of the large FOV, the optical point-spread-function (PSF) varies significantly over the focal plane, even at "best focus." The focus set point was chosen to attempt to minimize the diameter containing 95% of the PSF's encircled energy across the focal plane. However, the *Kepler* project was conservative in operating the focus mechanisms –one of the few moving parts in the spacecraft– and thus also wanted to minimize the number of focus adjustments. The spacecraft was launched with the mirror at the predicted in-flight best focus position, but once the photometer thermalized in-flight it was determined that the achieved point-spread function would result in being able to monitor only $\sim 130,000$ of the 170,000 stars for which the mission was designed. The final focus state was arrived at by two moves: a piston of 40 μm and a tip-tilt. The resulting 95% encircled energy diameters range from 3.2 to 7.5 pixels. Seasonal temperature variations of the photometer result in changes of up to $\pm 10\%$.[9]

2.1 Transmission and Quantum Efficiency

In order to meet its precision requirement of 20 ppm, the *Kepler* photometer needs to collect 4.6×10^9 electrons in 6.5 hours from a 12^{th} magnitude star. This precision requirement set the aperture size, transmission and quantum efficiency (QE) requirements for the photometer. Based on measurements of the Sun, a noise level of 10 ppm relative to a 12^{th} magnitude star has been allocated to stellar variability.

The *Kepler* focal plane consists of 21 modules, each with one field-flattener lens, which serves as the bandpass filter, and two CCDs. *Kepler's* focal plane average transmission curve is shown in Figure 1, along with the relative variation in integrated transmission for each of the 42 CCDs. The in-flight mean flux for 12^{th} stars is 4.59×10^9 electrons in 6.5 hours,[7] within 1% of the pre-launch prediction. The transmission curves in Figure 1 do not include geometric vignetting, which is less than 1% within 4.6 degrees of the center and increases to 11% at the edge of the FOV at 6.94 degrees off-axis. While the vignetting is independent of wavelength, there is color dependent variation over the focal plane caused by differences among the bandpass filters on the FFLs and by differing CCD QE. The mean CCD QE is shown in Figure 2a. A measure of the color-dependent variation in QE

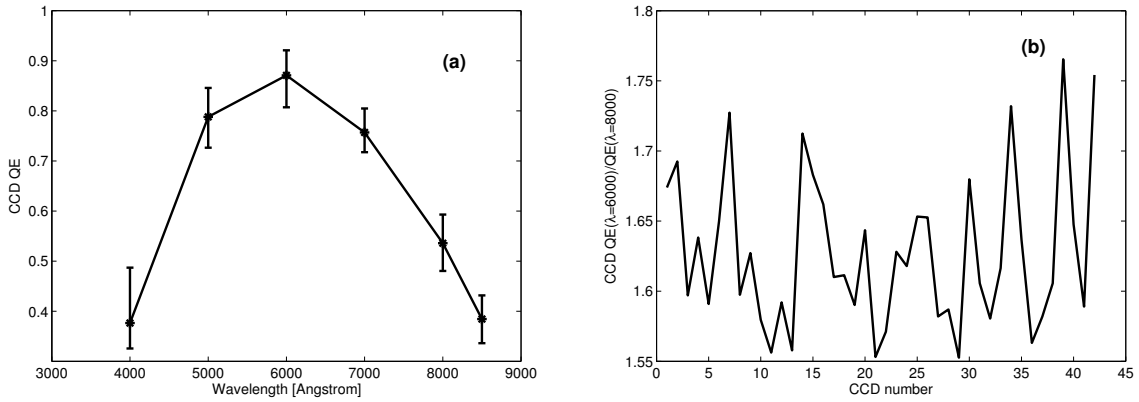

Figure 2: *Kepler* CCD QE over all CCDs on the focal plane. Panel (a) – mean QE over all CCDs. The error bars give the full range (max-min) of QE at each measured wavelength. Panel (b)– ratio of QE(6000Å)/QE(8000Å). The ratio varies from the mean ratio of 1.63 by −5% to +8% with an rms scatter of 3%.

is given in Figure 2b, which gives the ratio of QE at 6000 Å to the QE at 8000 Å. These wavelengths correspond roughly to the emission peak wavelength of a G5 star (T = 4800 K), and an M0 star (T = 3600 K); therefore, variations in the QE ratio of order 5% give an indication of the variations in relative response between G and M stars over the focal plane.

2.2 Scattered Light and Ghosting

Scattered light and ghosting generate optical crosstalk between stars on the focal plane and serve as a noise source in *Kepler* data. The levels of several scattered light and ghosting signals were modeled and measured prior to launch and were expected to be low enough to meet *Kepler's* precision requirements over 99% of the field of view. The most significant scattering and ghosting signals are given in Table 1, along with the log of the ratio of the scattered light/ghost signal to the source. Multiply the values by 2.5 to convert to astronomical magnitudes.

Table 1: Major scattered light and ghosting sources and relative signal levels.

Scattering/Ghost Source	**$\log_{10}$ of relative signal**
light scattered from the telescope structure (from objects in the FOV, or from objects outside the FOV –primarily Jupiter and the Earth)	-6 *predicted*
light scattered from the gaps between modules on the focal plane	-8.9
light scattered from the gaps between the CCDs on a module	-5.4, *predicted*
light scattered from the surface of the aluminum mask over the first 20 rows of each CCD	-4.3
specular scattering from the edge of the CCD	-4.5
specular scattering from the edge of the aluminum mask	-3.8
FFL surface ghosts	-5 per pixel, -2 integrated
Schmidt corrector ghost	-3.4

Objects outside the FOV scatter light diffusely over the entire focal plane. The combined signal from Earth and Jupiter was expected to be lower than 23.3 e^- $pixel^{-1}$ sec^{-1}, or less than 1 ppm for a magnitude 12 target

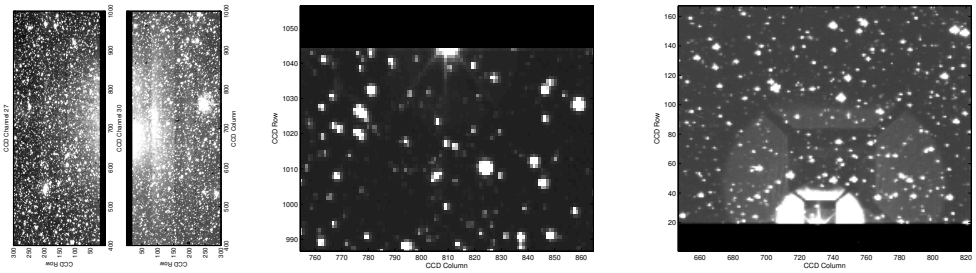

Figure 3: Scattered light from features on the focal plane: (a) Scattered light from the 4^{th} magnitude variable star 13 Lyr located in the gap between module 9 and module 10, *left panel*. Sections from the two affected CCD output channels are shown oriented as they appear on focal plane. The scattered signal peaks at about 60 e^- sec^{-1} $pixel^{-1}$, a factor of 2×10^{-7} times the source flux of 2.8×10^8 e^- sec^{-1} from 13 Lyr. However, the diffuse scattered light is spread over more than 100,000 pixels. (b) Scattered light from CCD edge at the gap between two CCDs on module 8, *middle panel*. The scattered signal can be seen near row 1044 and column 810. In this case, the peak scattered pixel is saturated, but the scattering signal's morphology is comparable to that from a point source; hence this scattering mode has very little impact on the FOV. (c) Scattered light from the CCD aluminum mask, *right panel*. The scattered signal appears much like the FFL ghost image from a star on the focal plane (Figure 4), since the aluminum mask is on the CCD surface under the FFL.

star. The scattered light from sources outside of the FOV has not yet been measured in flight, but with more than a year of data now available, we should be able to separate the scattered light signal from zodiacal light and other diffuse background sources.

Three of the focal plane scattering types are observed in flight as shown in Figure 3. Two of them –scattering from the CCD edge and scattering from the aluminum mask over the first 20 rows of each CCD– produce relatively local signal that can be quite intense. Because the scattering is off of an edge for these sources, the levels depend sensitively on the precise location of the scattering source. The third scattering type shown – scattering from the gaps between focal plane modules– produces a diffuse signal over a wider area of the focal plane. The largest observed signal is ~ 60 e^- sec^{-1} $pixel^{-1}$, or $\sim 2 \times 10^{-7}$ times the source signal (log of ratio = -6.7). In addition to being modulated by pointing changes, these scattering signals will be modulated by the variability of the source stars. While this effect has not been measured for any *Kepler* targets, it is expected to be a source of noise for some fraction of the FOV, based on the extent of the scattered light signal around the edge of the CCDs.

There are three optical ghosts that produce a significant signal on the *Kepler* focal plane (see Figure 4): (1) a reflection off of the CCD surface, off the back (nearest the CCD) surface of the FFL and back to the CCD, (2) off the CCD surface, off the FFL front surface and back to the CCD, and (3) reflection off of the CCD, off of the Schmidt corrector and back to a CCD across the focal plane.

In Quarter-1, the star shown in Figure 4 (Kepler 9528112) had a measured flux of 6.2×10^7 e^- sec^{-1}, corresponding to a measured Kepler magnitude of 5.8 (the star has a Kepler Input Catalog Kepler magnitude Kp=6.8). The total flux in the FFL ghost is $\sim 2\%$ of the source flux, but it is spread over approximately 2000 pixels, so the ghost flux per pixel is $\sim 1 \times 10^{-5}$ times the source flux. The ghost off of the front surface of the FFL is spread over nearly twice the area of the back surface ghost and is thus considerably fainter and only detectable for the few brightest stars on the focal plane. This front-surface ghost can be seen in the rightmost panel of Figure 3 as a larger fainter image of the central obscuration. The ratio of the flux in the Schmidt corrector ghost to the source flux in this image is $\sim 4 \times 10^{-4}$, or a log ratio of -3.4, compared with the pre-launch measure of -3.9.

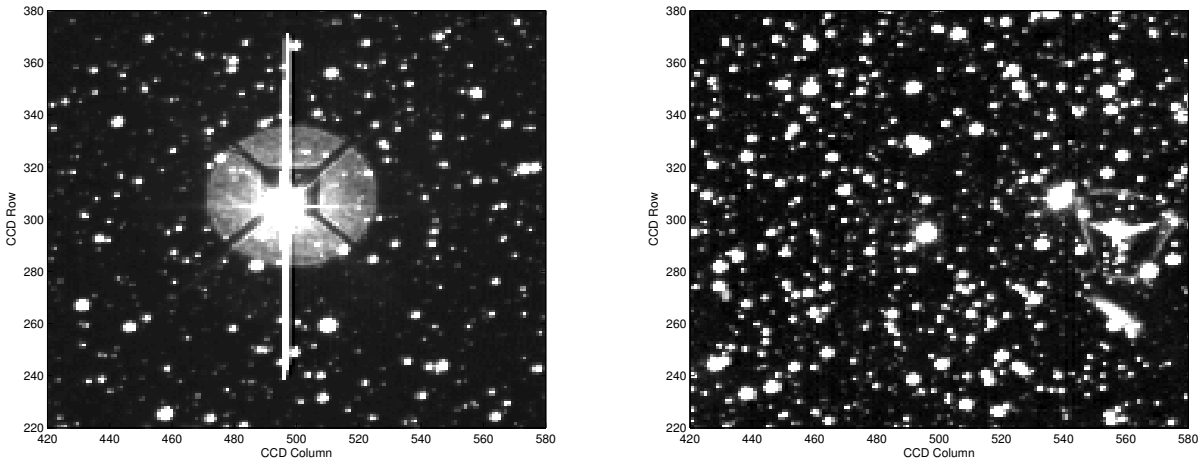

Figure 4: Sample optical ghost images: (a) FFL ghost seen around a bright star (Kepler 9528112, V* AF Cyg), left panel, and (b) Schmidt corrector ghost across the focal plane caused by this same star (centered around row, column = (300,560)), right panel. The visible FFL ghost is off of the back surface of the lens. It is spread over $\sim$ 2000 pixels and clearly shows an image of the central obscuration and support spider. The ghost off of the front surface of the FFL is not visible for this source. The Schmidt corrector ghost has a trefoil shape, indicating that the corrector plate is likely under some stress. This ghost is not exactly symmetrical across the focal plane but rather has a 60 pixel, or 4 arcmin, offset for this pair of channels due to slight variations in locations and orientations of the individual focal plane modules.

2.3 Background Flux

The background flux seen by *Kepler* comes primarily from two sources: zodiacal light from the solar system and diffuse starlight from faint background stars. The pre-launch predictions of the background level used a value of 334 e^- sec^{-1}, based on an assumption that the zodiacal light plus diffuse star background light is equivalent to one 22^{nd} magnitude star per square arcsecond.

In order to measure the background level, the *Kepler* project places $\sim$ 4400 pixels in 2×2 apertures in an approximate grid on each of the 84 detector channels. The background observations are taken at the long cadence rate.The background level for a given star is determined from a 2D polynomial fit to the measured background pixel values. Observations since *Kepler's* launch show that there are comparable background contributions from the zodiacal and Galactic sources. For a given instant in time, the measured background flux varies smoothly as a function of Galactic latitude (see Figure 5).In Quarter-3 (*Kepler's* Fall roll orientation), the background values range from 140e^- sec^{-1} to 250 e^- sec^{-1}, or $\sim$ 7 to 14 Digital Number (DN)/ read. While in Quarter-4 the background ranges from 190 to 330 e^- sec^{-1}, or $\sim$ 10 to 18 DN/read. The time variation of the background level for one sky location is dominated by the changing zodiacal light as *Kepler* orbits the sun. The time varying signal near the center of the FOV varies from 156 to 250 e^- sec^{-1}, as seen in Figure 6. The variation of $\sim$ 50 e^- sec^{-1} seen in Figure 5 for this location (the corner of the center module nearest the Galactic plane) between Quarter-3 and Quarter-4 can be accounted for by the difference in the time varying zodiacal signal, which has a peak-to-peak variation of $\sim$ 90 e^- sec^{-1} on a mean signal of 180 e^- sec^{-1}.

3. FOCAL PLANE ARRAY PERFORMANCE

3.1 Gain and Linearity

Kepler's gain and linearity were measured during ground testing using the photon transfer method with flood illumination.[3] The measured gain values for each are given in the *Kepler* Instrument Handbook and range from

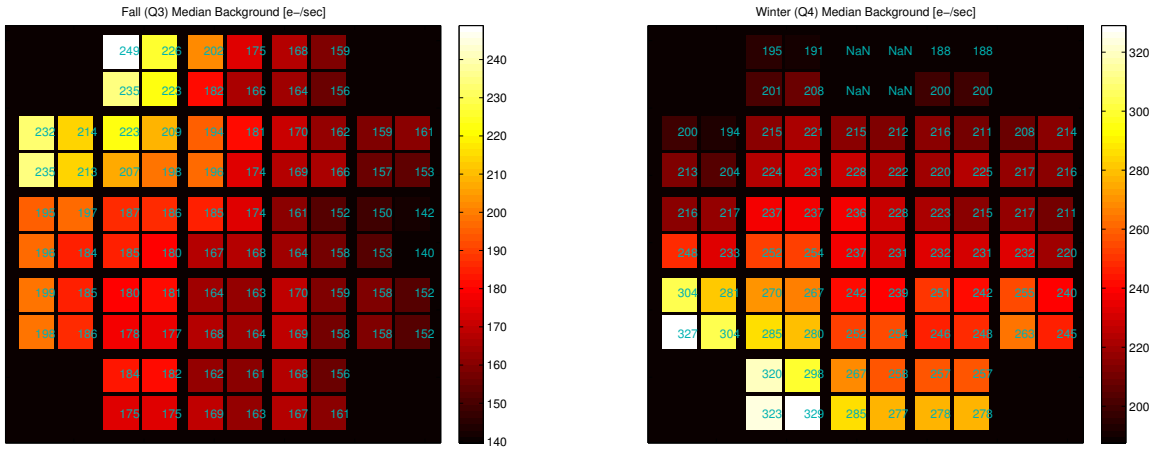

Figure 5: Median Background level measured over the focal plane for two different orientations of the photometer in e^-/s (a) Fall 2009 (Quarter-3), left panel and (b) Winter 2009/2010 (Quarter-4), right panel. The median over time of the background flux value for each output channel is shown in units of electrons/sec. In Quarter-3, the Galactic plane is oriented near the upper left of the focal plane. In Quarter-4 the Galactic plane is oriented near the lower left of the focal plane. Note that Module-3 (top row center) failed during Quarter-4, so there are no valid background measurements for this module. The layout of the channels on the focal plane can be found in the Kepler Instrument Handbook.[4]

93.5 e^-/DN to 120 e^-/DN.[4] Using this ground-based data, we have derived a pixel-level linearity correction that is applied during calibration. Determining the nonlinearity of the system is complicated by the difficulty in separating pixel-level nonlinearity from the onset of saturation.[10] In order to work around this difficulty, we determined the signal level of the onset of charge bleeding and the maximum signal level for each detector channel and then fit the differential photoresponse over non-saturating region with a polynomial that was constrained to go through the maximum signal level and have a derivative of zero at that point. The resulting nonlinearities determined from this procedure range from +3% to -4%.

In-flight measurement of the linearity of the *Kepler* CCDs is complicated by the limited range of exposure times available and the scientific requirement to maintain a continuous homogenous data set. Using bright variable stars, we see some evidence that the nonlinearity at the aperture level is much lower than the measured 3%, but we have yet to update the ground-based linearity measurements.

3.2 Crosstalk

There are two primary forms of electronic crosstalk on the *Kepler* focal plane: clock signal to video crosstalk and video to video crosstalk. Because the pattern of clock crosstalk signals is fixed on the pixels and the signals don't resemble star images, they can add noise, but aren't likely to generate false transit-like signals. The video to video crosstalk signals can be more problematic as they are star images and include all of the variability inherent in any given star. In addition, because we don't record data from all the stars on the focal plane, it is unlikely that we would have a direct measure of a target causing a problematic crosstalk signal.

3.2.1 Clock to Video Crosstalk

The clock to video crosstalk includes both FGS clock crosstalk into the science video and science clock crosstalk into the FGS module video. Because the readout of both the FGS and science modules is synchronized, the pixel locations of the crosstalk signals are deterministic. The science clock to FGS video crosstalk is mitigated in the attitude control system on board. The FGS clock to science video crosstalk generates a signal up to 10

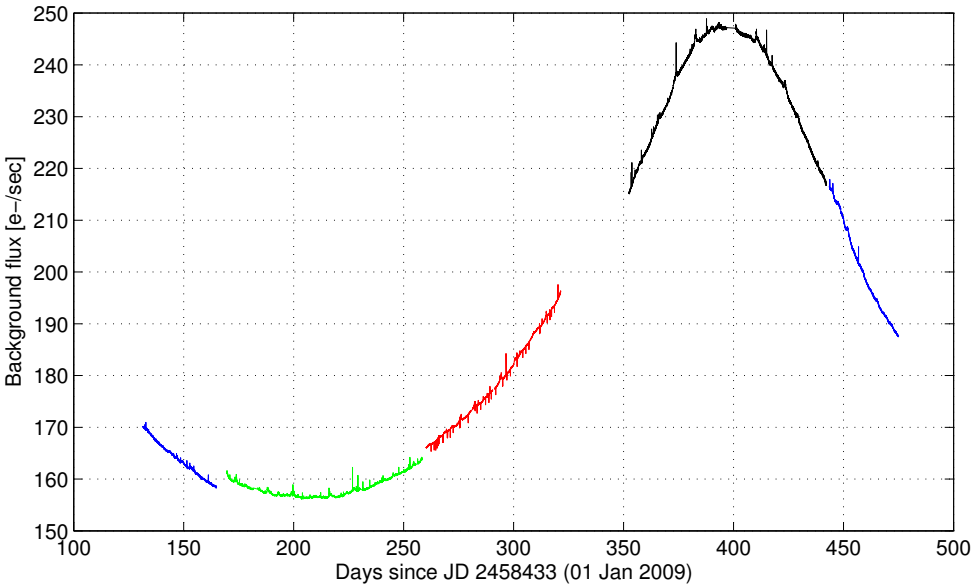

Figure 6: Time variation of Background level for a fixed sky location. The observations include approximately one year of background measurements from the central module in the focal plane, centered near ra, dec = ($19^{\mathrm{h}}27^{\mathrm{m}}$, $+44°30'$). The data from each roll orientation are indicated by color: Spring – blue, Summer – green, Fall – red, Winter – black. The seasonal variation is due to the changing zodiacal light signal as *Kepler* orbits the Sun and the angle between the Sun and the FOV changes. There are slight discontinuities at the seasonal rolls, because the data from the same portion of the sky are being collected on a different detector channel. Note that the background metric data are missing from the third month of the Fall orientation (near day 350). These data were successfully collected, but the background metrics were not calculated.

DN/read in the science data. Because its pattern is fixed on the science pixels and the level is mostly constant, we can remove the signal using a static two dimensional black, or bias, image. However, the crosstalk signals do show some temperature dependence, leaving a low level residual signal. The levels and impact of the FGS clock crosstalk have been covered elsewhere[3–5] and we have developed an algorithm for mitigating the thermally dependent crosstalk signals.[8]

3.2.2 Video to Video Crosstalk

Intramodule video to video crosstalk is seen between the four detector channels within a module on all science modules on the focal plane. The levels were first measured during ground testing where the maximum signal was found to be -46dB, or a factor of 200 attenuation, corresponding to 5.75 stellar magnitudes.[3] No intermodule video crosstalk was detected during ground testing, or so far in flight.

The four detector channels within a science module are read out synchronously, so that when a pixel from a given row and column is being read out on one channel, the pixels from the same row and column on each of the three other channels are also being read. Figure 7 shows a portion of four channels from module 3 showing particularly strong crosstalk. In order to measure the video crosstalk in flight, we measured the pixel flux from bright stars on a given source output channel and looked at the signal from the corresponding pixels on the other channels within that module. Our model of the crosstalk relies on four assumptions:

1. the crosstalk from one channel to another is linear, $\hat{s}_{ij} = C_{ij} S_j$,
2. the crosstalk coefficient, C_{ij}, is a constant over all pixels for a given source–recipient channel pair,

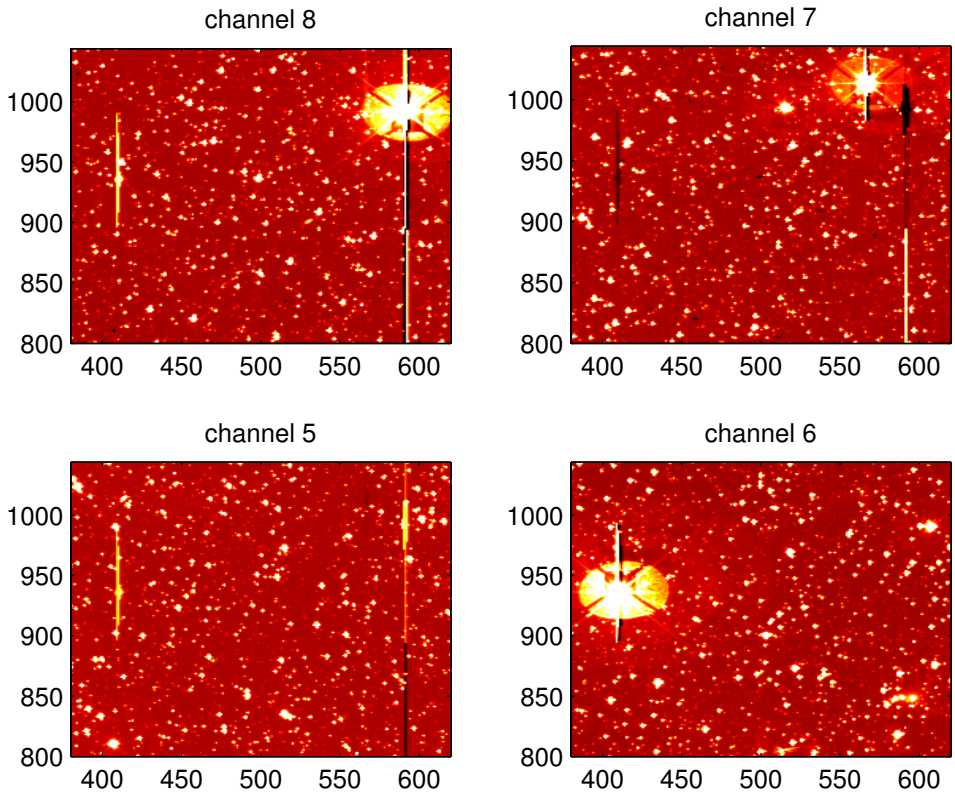

Figure 7: Video crosstalk on module-3. The four panels represent each of the four channels on module 3. Crosstalk from the bright star in channel 8 can be seen as a positive image in channel 5 and negative in channel 7, but is not detectible in channel 6. Crosstalk from the bright star in channel 6 produces positive signals in both channels 5 and 8, and a negative signal in channel 7. These results are consistent with the signs and magnitudes of the crosstalk coefficients for module 3 given in Table 2.

3. the total crosstalk in channel i is the simple sum of the crosstalk signals from all other channels $j \neq i$ on that module, $\hat{s}_i^{tot} = \sum_j^{j \neq i} \hat{s}_{ij}$, and

4. for any given pixel, no more than one of the four channels within a module will have a bright source on that pixel.

The notation used here is that S_j is the source pixel flux on detector channel j, C_{ij} is the coefficient for crosstalk from channel j to channel i, $\hat{s}_{ij}$ is the crosstalk signal on channel i due to a source on channel j, and $\hat{s}_i^{tot}$ is the total crosstalk signal on channel i. There will be one value of $\hat{s}_i^{tot}$ for each pixel on channel i, whose level depends on the source fluxes on the corresponding pixel from the three other channels on the same module.

Despite the large number of stars in the *Kepler* FOV, most of the pixels do not contain a detectable star, so in most cases, the pixels from a bright star on one channel do not overlap those of a bright star on another channel, simplifying our ability to measure C_{ij} by allowing us to consider only one source–recipient pair at a time. The approach we used was to assume that after removing the black (bias) signal, the dark current, and the sky background, the flux in any pixel for a given channel i is

$$S_i = S_{\rm star} + \hat{s}_{ij}, \tag{1}$$

where S_i is the measured signal in DN, $S_{\rm star}$ is the flux due to stars on channel i, and $\hat{s}_{ij}$ is the crosstalk signal defined above. Substituting for $\hat{s}_{ij}$ and dividing by the total crosstalk source signal, S_j allows us to solve for the crosstalk coefficient,

$$C_{ij} = S_i/S_j - S_{\rm star}/S_j. \quad (2)$$

Now if we select only pixels where the source image j is very bright and the recipient image i is dim, we can make the second term in Equation 2 small (< 0.002) and the crosstalk coefficient from channel j to channel i is simply the ratio of the images in these selected pixels. Since we are left with many hundreds of pixels meeting our selection criteria, we use the median of the C_{ij} values measured for each pixel for a given source–recipient channel pair as a robust estimate of the true crosstalk coefficient. This procedure minimizes the impact on our estimate of C_{ij} of the rare cases where two bright stars on different channels within a module fall on the same pixels. The resulting crosstalk model consists of 12 crosstalk coefficients for the four channels on each of the 21 modules for a total 252 coefficients. Note that the crosstalk coefficients can be either positive or negative and that in general $C_{ij} \neq C_{ji}$.

Table 2: Crosstalk coefficients, C_{ij} for module 3. Note the table is not symmetric in sign or magnitude. This array is a subset of the full 252 element crosstalk coefficient array for the entire focal plane.

Recipient channel	**ch 5 source**	**ch 6 source**	**ch 7 source**	**ch 8 source**
5	0	5.2×10^{-4}	-3.4×10^{-5}	6.2×10^{-4}
6	5.6×10^{-4}	0	4.5×10^{-5}	3.4×10^{-5}
7	6.5×10^{-6}	-1.6×10^{-4}	0	-2.5×10^{-3}
8	-5.6×10^{-4}	7.0×10^{-4}	1.3×10^{-4}	0

The coefficients can be represented in an 84×84 block diagonal matrix, where each module is represented in 4×4 sub-matrices. Using this formulation, a total crosstalk image for a given channel can be obtained by multiplying the images from the other 3 channels within the module by the coefficient matrix. We will use this crosstalk model to check for cases where there are significant contaminating crosstalk signals falling on a target of interest.

3.3 Noise

One of *Kepler's* driving requirements is the photometric precision measured on timescales of the transits of most interest to the Mission goals: Earth-size transits of a a sun-like star in a habitable zone orbit. At the orbital distance of the Earth, a central transit on a G2 dwarf star takes 13 hours. A transit with an impact parameter of $0.866R_*$ has a duration of one-half that of a central transit, or 6.5 hours. *Kepler* was designed to achieve a 4σ detection on an Earth-size transit of a 12^{th} magnitude G2 dwarf in 6.5 hours, or a precision of 20 ppm. This design goal set the aperture size –Poisson noise is the largest noise component at 12^{th} magnitude, the read noise requirements, the duty cycle requirements, as well as the stray light, background, and pointing jitter induced noise requirements. This precision metric is a combination of all instrument and sky noise sources, including an assumed 10 ppm stellar variability term, and is a differential measure of changes on timescales of 6.5 hours. It is referred to as the combined differential photometric precision (CDPP).

Kepler's instrument noise contributions were measured during pre-launch testing, where two channels were found to have consistently high read noise that put them above the limit (< 150 e $^{-1}$/read) to achieve 20 ppm CDPP. They were predicted to have CDPP levels of 21 ppm and 20.1 ppm for channel 3.3 & 24.3 respectively. Three other channels were found to exceed the read noise allocation in some tests, but not others.[3] The unstable noise measurements are caused by moire pattern image artifacts that lead to portions of the channel being above the 20 ppm limit. Several other channels also showed significant pattern noise under certain thermal conditions. During operations, the noise that is associated with image artifacts has been observed at levels higher than seen on the ground in some channels. The excellent thermal stability of the photometer has also allowed us to detect these image artifacts in several channels not noted during ground tests.[5, 8]

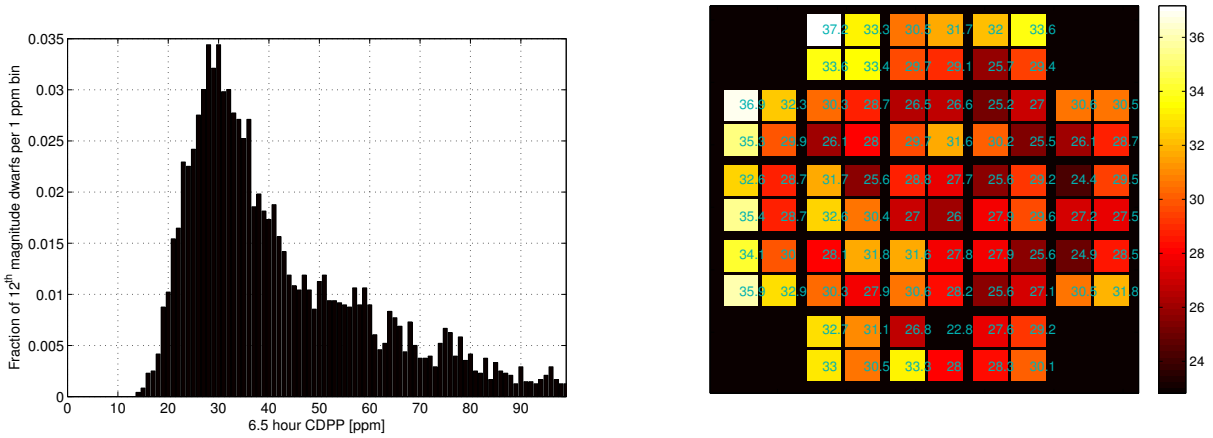

Figure 8: Combined differential photometric precision at 6.5 hours from Quarter-3 for all dwarf stars with $11.5 <$ Kepler Mag ≤ 12.5: (a) histogram of the distribution, left panel, and (b) the 25^{th} percentile of the distribution on each detector channel. The 12^{th} magnitude CDPP requirement is 20 ppm at 6.5 hours. Dwarf stars were selected using a surface gravity cutoff since sub-giants and giants are significantly more variable and thus their noise would be dominated by stellar variability. Approximately 10% of the 12^{th} magnitude dwarfs are noisier than 100 ppm. The 25^{th} percentile was used as an empirically determined proxy for the mode of the distribution.

In order to judge the performance of the photometer, the Science Operations Center (SOC) pipeline processing calculates the measured precision at 3, 6, and 12 hour timescales for every star.[11,12] The median CDPP for 12^{th} magnitude dwarf stars measured in Quarter-3 is 39.5 ppm. The 25^{th} percentile of the distribution (approximately the mode) is 29 ppm. The distribution of CDPP and it's dependence on focal plane position are shown in Figure 8. The distribution of the 25^{th} percentile of CDPP across the focal plane is strongly correlated with the background level on the channel (see Figure 5a), with a correlation coefficient of 0.6. The correlation is even stronger between the CDPP and background $\times$ star image diameter, with a correlation coefficient of 0.73, indicating that the interaction of faint background stars with the edge of the aperture may be a driving factor in limiting our precision. The excess noise is red, as our precision on shorter time scales is much closer to predictions: the measured noise at frequencies greater than 5 cycles/day has a mode of 22 ppm.[7] We are currently conducting a number of studies to pinpoint the causes of the higher-than expected CDPP. We can't yet rule out that stellar variability is higher than the allocated 10 ppm at 6.5 hours, but given the distribution of CDPP over the focal plane, there must be some instrumental contribution as well. Also, given that we do have some stars at or below the 20 ppm noise level, we are confident that the photometer is capable of performing as well as expected and are hopeful that improvements in data processing will increase the number of stars meeting our pre-launch expectations.

4. SUMMARY

The *Kepler* instrument properties and performance in the first year of operations are consistent with pre-launch test results, though the excellent stability of the photometer has allowed us to uncover some unexpected behavior. Flux levels from stars are very close to predictions, indicating that the optical transmission and CCD QE are as expected. Scattered light and ghost signals have been measured at a somewhat higher level then predicted; however their limited extent on the focal plane will not cause a problem with meeting the mission goals. CCD gain, linearity, and saturation behavior is proving more complex than expected and there are indications that our pre-launch models don't correctly describe the photometer's behavior. While these properties do not strongly impact our ability to meet the mission goals, they can be significant for bright stars, so we are working to update the models based on flight data. Electronic crosstalk signals are at levels measured on the ground. The

predominance of video crosstalk could present a confusion problem for some targets, so we have developed a model that allows us to check targets of interest against potential crosstalk signals. Finally, one of the driving requirements for *Kepler*, photometric precision, is somewhat worse than expected. We find that the instrument is meeting precision requirements at short timescales (> 5 cycles/day), but red noise is resulting in increased CDPP at 6.5 hour timescales. There is evidence that at least part of this increase is due to the instrument and/or data processing, as the noise levels show significant correlation with focal plane properties, in addition to the sky background level. We are currently working to understand the source of the increased red noise.

ACKNOWLEDGMENTS

We gratefully acknowledge the years of work by the many hundred members of the Kepler Team who conceived, designed, built, and now operate this wonderful mission. Funding for the *Kepler Mission* is provided by NASA's Science Mission Directorate.

REFERENCES

1. Koch, D. G. *et al.*, "*Kepler* mission design, realized photometric performance, and early science," ApJ Lett. 713(2), L79-L86 (2010).
2. Borucki, W. J. *et al.*, "*Kepler* planet-detection mission: introduction and first results," Science 327, 977-980 (2010).
3. Argabright, V. S. *et al.*, "The *Kepler* photometer focal plane array," Proc. SPIE 7010, 76 (2008).
4. Van Cleve, J., & Caldwell, D. A. 2009, "Kepler Instrument Handbook, KSCI 19033-001," NASA Ames Research Center: `http://archive.stsci.edu/kepler/`
5. Caldwell, D. A. *et al.*, "Instrument performance in *Kepler's* first months," ApJ Lett. 713(2), L92-L96 (2010).
6. Borucki, W. J. *et al.*, "*Kepler's* optical phase curve of the exoplanet HAT-P7b," Science 325, 709 (2009).
7. Jenkins, J. M. *et al.*, "Initial characteristics of *Kepler* long cadence data for detecting transiting planets," ApJ Lett. 713(2), L120-L125 (2010).
8. Kolodziejczak, J. *et al.*, "Flagging and correction of pattern noise in the *Kepler* focal flane frray," Proc. SPIE 7742, in press (2010).
9. Bryson, S. T., *et al.* "The *Kepler* pixel response function," ApJ Lett. 713(2), L97-L102 (2010).
10. Gilliland, R. L., Goudfrooij, P., & Kimble, R. A. "Linearity and High Signal-to-Noise Performance of the STIS CCD," PASP 111, 1009 (1999)
11. Jenkins, J. M. *et. al.*, "Transiting planet search in the Kepler pipeline," Proc. SPIE 7740, in press (2010).
12. Li, J. *et. al.*, "Photometer performance assessment in *Kepler* science data processing," Proc. SPIE 7740, in press (2010).